The Journal of Chemical Physics

RESEARCH ARTICLE | NOVEMBER 10 2026

Quantum-classical hierarchical equations of motion

Amartya Bose

Check for updates

J. Chem. Phys. 165, 184107 (2026)
https://doi.org/10.1063/5.0361587

View Online
Export Citation

Articles You May Be Interested In

QuantumDynamics.jl: A modular approach to simulations of dynamics of open quantum systems
J. Chem. Phys. (May 2023)

Quantum-classical path integral with a harmonic treatment of the back-reaction
J. Chem. Phys. (May 2019)

Iterative quantum-classical path integral with dynamically consistent state hopping
J. Chem. Phys. (January 2016)

15 November 2026 03:50:56

AIP Publishing
The Journal of Chemical Physics
Special Topics Open for Submissions
Learn More

AIP Publishing

The Journal of Chemical Physics ARTICLE pubs.aip.org/aip/jcp

Quantum-classical hierarchical equations of motion

Cite as: J. Chem. Phys. 165, 184107 (2026); doi: 10.1063/5.0361587
Submitted: 21 September 2026 • Accepted: 26 October 2026 •
Published Online: 10 November 2026

View Online Export Citation CrossMark

Amartya Bose[a)]

AFFILIATIONS

Department of Chemical Sciences, Tata Institute of Fundamental Research, Mumbai 400005, India

[a)]Author to whom correspondence should be addressed: amartya.bose@tifr.res.in and amartya.bose@gmail.com

ABSTRACT

We develop a quantum–classical hierarchical equations of motion (QC-HEOM) approach for simulating non-Markovian open quantum systems. The method combines the ensemble-averaged classical path reference of the quantum–classical path integral formalism with a hierarchy of auxiliary quantum influence functionals. By incorporating thermal fluctuations through an ensemble average over reference trajectories, the hierarchy is required to represent only the residual quantum memory associated with the imaginary part of the bath response function. Consequently, unlike conventional hierarchical equations of motion, QC-HEOM does not require Matsubara or Padé expansions of the thermal kernel and exhibits only weak temperature dependence of the hierarchy size. Furthermore, because thermal fluctuations are supplied through reference classical trajectories, the framework provides a natural route toward extensions beyond harmonic baths and enables the incorporation of anharmonic and molecular environments through externally generated trajectories. We derive the QC-HEOM formalism and demonstrate its exactness for a harmonic bath. Applications to an asymmetric spin–boson model and an eight-site model of the Fenna–Matthews–Olson complex illustrate the accuracy of QC-HEOM. It reproduces benchmark exact quantum dynamics results while requiring substantially fewer auxiliary objects, particularly at low temperatures. These results establish QC-HEOM as an efficient framework for treating residual quantum memory in quantum–classical descriptions of open-system dynamics. The separation of thermal fluctuations from residual quantum memory through the use of Wigner trajectories suggests an approximate route toward hierarchical treatments of complex anharmonic environments beyond harmonic bath simulations, which shall be developed in the future.

Published under an exclusive license by AIP Publishing. https://doi.org/10.1063/5.0361587

15 November 2026 03:50:56

I. INTRODUCTION

The numerical challenges of simulating the time-evolution of a quantum system under the Schrödinger equation scale exponentially with dimensionality. In systems such as exciton- or charge-transfer, it is often seen that the actual event of interest is actually localized within a much smaller dimensional Hilbert space, with the other degrees of freedom modulating the dynamics. This realization has led to a variety of methods that develop a system-environment decomposition, where the environment is traced out, leading to a non-Markovian equation of motion.

Two broad classes of methods exist within the system-environment decomposed approaches. First, we have the category of numerically exact methods, which can only be applied to the case of the environment being represented as harmonic baths. The family of quasi-adiabatic propagator path integral methods (QuAPI),[1–7] based on the Feynman–Vernon influence functional[8] and the methods related to the hierarchical equations of motion (HEOM)[9–17] are two of the most well-known exact methods in the community. From their inception more than three decades ago, these two methods have become the standard for benchmark applications and accuracy. The main shortcoming of these methods has historically been their extraordinarily high cost and complexity. Several algorithmic improvements have made their application to simulation of large systems possible.

The other category comprises the ubiquitous mixed quantum–classical methods, which relegate the treatment of the environment to classical trajectories and evolve the system using approximate quantum mechanics in response to these trajectories. The earliest mixed quantum–classical method is probably Ehrenfest dynamics or self-consistent field dynamics. Approaches based on surface hopping dynamics[18–21] are also extremely popular

Published under an exclusive license by AIP Publishing

for approximating the non-adiabatic evolution of systems. The quantum–classical path integral (QCPI)[22,23] provides a rigorous and systematic way of approximating the path integral results using (quasi-)classical trajectories for anharmonic systems. While approximate for anharmonic systems, QCPI is exact in the limit of harmonic baths and reduces to the harmonic Feynman–Vernon influence functional[8] results.

Under QCPI, the system's reduced density matrix is written as an environment phase space integral of the so-called "quantum influence function," which is evaluated as a path integral with free solvent-driven reference propagators.[24] Makri showed that these reference propagators, also called the "ensemble averaged classical path" (EACP) reference propagators, themselves account for the "classical memory" corresponding to the real part of the bath response function.[25] The path integral incorporates the "quantum memory." It has also been suggested that restricting the full anharmonic trajectories for the reference propagator part and approximating the quantum memory using the harmonic mapping can be a convenient approximation that avoids exponential proliferation of classical trajectories while keeping the path integral with analytical influence functional coefficients.[26,27]

Despite these improvements, QCPI still requires path integral simulations for every Monte Carlo sample of the solvent phase space. This can, depending on the parameters, be quite computationally intensive. On the other hand, the application of HEOM to non-adiabatic dynamics, even with all the developments, is limited to bosonic or fermionic baths (For anharmonic vibrational problems, a HEOM-like quantum hierarchical Fokker–Planck equations[15] can be used under the Wigner approximation. However, this is no longer exact at a quantum level even for the system and is effectively semiclassical). In this work, we present a combination of the two ideas, where, as in QCPI, the classical memory is accounted for by solvent-driven references; however, the quantum memory is incorporated using HEOM. This avoids the path integral calculation altogether leading to better scaling. Additionally, the number of poles required for the HEOM calculation is significantly reduced, because the real part of the bath correlation function is completely accounted for by the reference, thus avoiding the proliferation of poles required to represent the thermal Bose–Einstein distribution in the real part. This quantum–classical HEOM (QC-HEOM), unlike the hierarchical Fokker–Plank equations of motion,[15] manages to achieve this separation and consequent simplification while not introducing any semiclassical approximations for harmonic baths. For harmonic environments, QC-HEOM remains formally equivalent to the underlying QuAPI while replacing path-integral propagation with a hierarchical equation-of-motion treatment of the residual quantum memory.

Stochastic HEOM[16,17] provides another approach for treating the real part of the bath response function by introducing a stochastic unraveling through a Hubbard–Stratonovich transformation. Recent extensions have enabled the treatment of anharmonic baths by incorporating higher-order multitime correlation functions.[28,29] QC-HEOM follows a different philosophy. Rather than introducing an auxiliary stochastic field, it identifies the fluctuation contribution associated with the real part of the bath response function with the solvent-driven reference trajectories already present in the QCPI framework. The remaining dissipative contribution is treated hierarchically. The stochastic variables sampled in the two approaches are therefore fundamentally different: stochastic HEOM samples realizations of a Gaussian colored-noise field, whereas QC-HEOM samples initial conditions of physical bath trajectories from a thermal Wigner distribution. For harmonic baths, where the Hubbard–Stratonovich transform is valid because of Gaussian statistics, the two methods seem to give two different approaches of generating the same influence due to the bath. However, even at this level, because QC-HEOM works with Wigner trajectories, it enables more detailed incorporation of physics in them through bath references that are forced by the system.[24,30] Such references would help reduce the amount of the back-reaction that needs to be accounted for through the hierarchy, thus reducing the computational effort. This will be explored in the future. Similarly, through its connection to QCPI, QC-HEOM permits future extensions toward anharmonic or atomistic environments within the harmonic backreaction approximation in a very natural manner through the corresponding classical trajectories.

In Sec. II, we derive QC-HEOM from the fundamental path integral expressions and discuss how the reference trajectory formulation provides a possible extension toward anharmonic environments. Applications involving an asymmetric spin–boson system and an eight-site model for the Fenna–Matthews–Olson complex are used to demonstrate the correctness, performance, and convergence of QC-HEOM in Sec. III. It is seen that even relatively low depths of hierarchy suffice to give fully converged results, with the biggest correction happening from the EACP dynamics to the dynamics corresponding to depth 1. Additionally, the exponential representation of the bath response function used for QC-HEOM does not require explicit accounting of the thermal part, leading to a decrease in the number of terms. These two factors together make the method cheap and extremely lucrative for simulations. Finally, some concluding remarks and future directions are presented in Sec. IV.

II. METHOD

For simplicity of development, let us consider a system coupled with a bath of harmonic oscillators described by

$$H = H_0(\hat{s}) + H_{\mathrm{SB}}(\hat{q}, \hat{s}), \tag{1}$$

where H_0 is the system Hamiltonian and H_{SB} is the bath Hamiltonian (including the system-bath interaction terms). Using path integrals, one can express the time-evolved reduced density matrix corresponding to the system starting from a separable initial condition, $\rho(0) = \tilde{\rho}(0) \otimes \exp(-\beta H_{\mathrm{SB}})/Z_{\mathrm{SB}}$ as

$$\langle s^+(t)|\tilde{\rho}(t)|s^-(t)\rangle = \int \mathcal{D}[s^{\pm}(t)] e^{i(S[s^+(t)]-S[s^-(t)])/\hbar} \times \langle s^+(0)|\tilde{\rho}(0)|s^-(0)\rangle \mathcal{F}[s^{\pm}(t)], \tag{2}$$

where $s^+(t)$ is the forward path, $s^-(t)$ is the backward path, S is the classical action, and $\mathcal{F}$ is the Feynman–Vernon influence functional[8] that encodes the system–bath interaction and causes the dynamics to become non-Markovian in general. The influence

15 November 2026 03:50:56

Published under an exclusive license by AIP Publishing

functional, $\mathcal{F}$, for a harmonic bath can be expressed as the exponential of the "influence phase" $\exp\left(-\Phi\left[s^{\pm}(t)\right]\right)$ in terms of the bath response function, $\alpha(t)$,

$$\Phi\left[s^{\pm}(t)\right] = \int_0^t \mathrm{d}t' \int_0^{t'} \mathrm{d}t'' \Delta s(t') \Re\alpha(t'-t'') \Delta s(t'') - 2i \int_0^t \mathrm{d}t' \int_0^{t'} \mathrm{d}t'' \Delta s(t') \Im\alpha(t'-t'') \bar{s}(t''), \quad (3)$$

where $\Delta s(t) = s^+(t) - s^-(t)$ and $\bar{s}(t) = \frac{1}{2}\left(s^+(t) + s^-(t)\right)$. While these expressions have been provided here in continuous time, if time is discretized and a symmetric Trotter splitting is used with the quasi-adiabatic split Hamiltonian, these expressions become identical to the ones used in the quasi-adiabatic propagator path integral method.[1,2] If the bath is characterized by a spectral density, $J(\omega)$, then

$$\alpha(t) = \frac{1}{\pi} \int_0^{\infty} \mathrm{d}\omega J(\omega) \left(\coth\left(\frac{\hbar\omega\beta}{2}\right) \cos(\omega t) - i \sin(\omega t) \right), \quad (4)$$

where $\beta = 1/k_B T$ is the inverse temperature for the simulation.

Quantum–classical path integral[22,23] (QCPI) by Makri and coworkers offers a way of estimating the influence functional for general environments using quasi-classical (Wigner) trajectories. The system's reduced density matrix at time t is given by

$$\left\langle s^+(t)|\tilde{\rho}(t)|s^-(t)\right\rangle = \iint \mathrm{d}q_0 \mathrm{d}p_0 P(q_0,p_0) \left\langle s^+(t)|Q_{q_0,p_0}(t)|s^-(t)\right\rangle, \quad (5)$$

$$\left\langle s^+(t)|Q_{q_0,p_0}(t)|s^-(t)\right\rangle = \int \mathcal{D}\left[s^{\pm}(t)\right] \left\langle s^+(0)|\tilde{\rho}(0)|s^-(0)\right\rangle \times e^{i\left(S_{\mathrm{ref}}\left[s^+(t);q_0,p_0\right] - S_{\mathrm{ref}}\left[s^-(t);q_0,p_0\right]\right)/\hbar} \exp\left(-\Phi_{\mathrm{back}}\left[s^{\pm}(t)\right]\right), \quad (6)$$

where P is the Wigner phase space density, and Q is the quantum-influence function. The reference action, S_{ref}, is the classical action of the system along a given path under the time-dependent Hamiltonian, $H_{\mathrm{ref}}(t;\ q_0,p_0) = H_0 + H_{\mathrm{SB}}(q(t;\ q_0,p_0))$, generated along the solvent reference trajectory, $q_{\mathrm{ref}}(t;\ q_0,p_0)$, with initial conditions (q_0,p_0). The modified influence functional is related to the reference-dependent residual back-reaction, Φ_{back}. The impact of temperature on the dynamics is captured purely through the Wigner phase space density and classical trajectories, and Φ_{back} is independent of temperature.

QCPI reproduces the exact influence functionals for the case of harmonic baths. If the reference trajectory is chosen to be the free solvent trajectory,

$$q(t;q_0,p_0) = q_0 \cos(\omega t) + \frac{p_0}{\omega} \sin(\omega t). \quad (7)$$

Then, it is known that the real part of the bath response function, or the classical memory, is completely accounted for even without incorporating the back-reaction.[25] This reference is called the ensemble-averaged classical path (EACP) reference, and the approximate dynamics is called the EACP dynamics.[24] Consequently, Φ_{back} becomes the part that simply comes from the imaginary part of the bath response function or the quantum memory.[25] This can be related to the imaginary part of the η-coefficients from QuAPI and the bath response function.[1,25]

For a molecular or anharmonic solvent, the general procedure is to solve for Φ_{back} using single classical trajectories for each of the system paths within memory. This exponential proliferation of the classical trajectories can be avoided under the harmonic backreaction approximation,[26,27] where one uses the anharmonic reference trajectories defined by

$$\dot{q}(t) = \frac{p(t)}{m}; \quad \dot{p}(t) = -\nabla V_{\mathrm{sol}}(q(t)), \quad (8)$$

where V_{sol} is the pure solvent environment to get the reference actions, but replaces the backreaction Φ_{back} with that of the equivalent harmonic mapping.

While the use of reference propagator significantly decreases the length of the effective non-Markovian memory and allows for the use of larger time-steps, even under harmonic backreaction, the path integral for the quantum influence function, Q, still has to be computed for each Monte Carlo sampled initial condition, (q_0,p_0). This can often be a major bottleneck, especially for large systems with long "quantum" memory.

This motivates the development of an alternative formulation that eliminates explicit path integral evaluation while retaining the full non-Markovian memory through a structured representation of the dissipative kernel. Since the residual backreaction influence functional depends only on $\Im\alpha(t)$, the quantum influence function $Q_{q_0,p_0}(t)$ has precisely the same structure as the reduced density matrix of a system would have, except the bath response function is formally replaced by the purely imaginary $C_{\mathrm{back}}(t) = i\Im\alpha(t)$. Additionally, the bare system evolution is now under the trajectory-dependent reference Hamiltonian, $H_{\mathrm{ref}}(t;\ q_0,p_0)$. Consequently, any exponential decomposition of $\Im\alpha(t)$ immediately gives rise to a hierarchy of auxiliary density operators identical in structure to the standard HEOM. In the present work, we therefore replace the path-integral evaluation of $Q_{q_0,p_0}(t)$ by propagation of the corresponding hierarchy and recover the physical reduced density matrix by averaging over the initial Wigner distribution.

Whenever $C_{\mathrm{back}}(t)$ admits an exponential representation, either exact or approximate, it can be written as

$$C_{\mathrm{back}}(t) = \sum_{m=1}^{M} c_m \exp(-\nu_m t), \quad (9)$$

where $\nu_m \in \mathbb{C}$ are the poles of the exponential representation of the residual bath response function. In the simplest case of a Drude–Lorentz spectral density, the poles are all real. In more general cases, that is not necessary. However, because the bath response function in general, and $C_{\mathrm{back}}(t)$ in particular, satisfies $C_{\mathrm{back}}(-t) = C^*_{\mathrm{back}}(t)$, all non-real poles occur in complex conjugate pairs. Rather than treat the real and the complex poles separately, we associate with each exponential mode tuples of three numbers, $(\nu_m, c_m, \tilde{c}_m)$, where ν_m and c_m correspond to Eq. (9). The third number $\tilde{c}_m$ is the coefficient corresponding to ν_m in the exponential expansion of $C^*_{\mathrm{back}}(t) = \sum_m c^*_m \exp\left(-\nu^*_m t\right)$. So if $\nu_m \in \mathbb{R}$, the $\tilde{c}_m = c^*_m$. However, if ν_m is complex and ν_n is its complex conjugate, then $\tilde{c}_m = c^*_n$. Using this, one immediately gets equations for the quantum influence function, $Q_{q_0,p_0}(t)$, that are formally similar to standard HEOM. We indicate the auxiliary quantum influence function (AQIF) of

15 November 2026 03:50:56

Published under an exclusive license by AIP Publishing

the **n**th level as $Q^{\mathbf{n}}_{q_0,p_0}(t)$. Using this notation now, we list the scaled HEOM-like equations[12] for QC-HEOM,

$$\dot{Q}^{\mathbf{n}}_{q_0,p_0}(t) = -\left(i\mathcal{L}_{\mathrm{ref}}(t;q_0,p_0) + \sum_{m=1}^{M} n_m \nu_m\right) Q^{\mathbf{n}}_{q_0,p_0}(t) - i\left[\hat{s}, \sum_{m=1}^{M} \sqrt{(n_m+1)s_m}\, Q^{\mathbf{n}^+_m}_{q_0,p_0}(t)\right] - i\sum_{m=1}^{M} \sqrt{\frac{n_m}{s_m}}\left(c_m \hat{s} Q^{\mathbf{n}^-_m}_{q_0,p_0}(t) - \tilde{c}_m Q^{\mathbf{n}^-_m}_{q_0,p_0}(t)\hat{s}\right), \tag{10}$$

where $s_m = \sqrt{|c_m \tilde{c}_m|}$. For purely real poles, this equation parallels the scaled HEOM equations of motion.[12] The exponential representation may be obtained analytically for several model spectral densities or numerically using rational approximation techniques such as the barycentric AAA algorithm.[13,31] Additionally, Eq. (10) is a series of coupled differential equations for each hierarchy level indexed by **n**. This hierarchy gets truncated at a particular depth indicated by L, which is a convergence parameter.

In Eq. (10), $\mathcal{L}_{\mathrm{ref}}(t;q_0,p_0)$ is the Liouvillian corresponding to the time-dependent reference Hamiltonian, $\mathcal{L}_{\mathrm{ref}}(t;q_0,p_0) = [H_{\mathrm{ref}}(t;q_0,p_0),\cdot]$. The time-evolution of the Wigner phase-space point (q_0,p_0) happens under the bath Hamiltonian. In the current work, the bath is taken to be harmonic, but this restriction can naturally be lifted, and Eq. (8) can be used to solve the classical equations of motion. This enables the reference Hamiltonian to incorporate the anharmonic effects of the bath approximately, and the consequences will be explored elsewhere.

The low temperature termination is conspicuously absent in Eq. (10), because the entire thermal component is taken into account through the classical trajectories. Here, the modes come solely from the poles for the spectral density and not from those of the Bose–Einstein distribution. In standard HEOM, the decomposition of the bath response function into exponential decays, Eq. (9), gives rise to an infinite set of Matsubara poles even when the poles of the spectral density are finite in number. This leads to a convergence problem especially at low temperatures when accurately representing the Bose–Einstein distribution becomes demanding. Various techniques like Padé fitting[32,33] have therefore been developed to reduce the number of poles required in practical calculations. In QC-HEOM, however, the hierarchy is constructed only from the residual backreaction kernel $C_{\mathrm{back}}(t) = \mathrm{Im}\,\alpha(t)$. Since $\mathrm{Im}\,\alpha(t)$ is independent of temperature, the thermal contribution contained in $\mathrm{Re}\,\alpha(t)$ is accounted for entirely through the ensemble of classical reference trajectories. Consequently, the Matsubara contribution never enters the hierarchy, trading one of the primary low-temperature bottlenecks of conventional HEOM in favor of a simulation of multiple trajectories. Therefore, as will be demonstrated in Sec. III, in contrast to standard HEOM, the hierarchy of QC-HEOM is only weakly dependent on the temperature.

The conceptual framework of QC-HEOM is naturally compatible with other recent developments of HEOM, including incorporation of tensor networks and free-pole formulation of HEOM.[13] The twin advantages of not requiring any Matsubara modes and being able to approximately capture the effect of anharmonic baths through classical trajectories are independent of the details of the hierarchy and only dependent on the reference propagators. Consequently, irrespective of the exact hierarchy and nature of poles, they will continue to hold. These will be the focus of future developments. QC-HEOM is similar to the stochastic HEOM method,[16,17] which stochastically unravels the classical memory by using a colored noise kernel $\xi(t)$. The Hubbard–Stratonovich transform restricts $\langle\xi(t)\rangle = 0$, and relates the two-time correlation function to the real part of the bath response function.[16] One of the most important differences here is that instead of an abstract colored noise kernel, QC-HEOM leverages insights from QCPI to relate the stochastic unraveling to linearized semiclassical or Wigner trajectories of the free solvent degrees of freedom.

III. NUMERICAL ILLUSTRATIONS

We will discuss application of QC-HEOM to the spin–boson model and an 8-site model of the Fenna–Matthews–Olson complex at a variety of temperatures. Comparisons will be shown with QCPI, QuAPI, and HEOM. In all QC-HEOM and QCPI simulations, a light shaded band of the same color indicates the standard error associated with the stochastic sampling of the Wigner trajectories. These uncertainties remain small for all systems and temperatures considered and are generally smaller than the linewidth, demonstrating that the number of reference trajectories used provides statistically converged ensemble averages for the benchmark systems studied here. All methods were used from the QuantumDynamics.jl package.[34] An open-source implementation of QC-HEOM will be released as a part of the next update to the framework.

A. Spin–boson system

Consider an asymmetric spin–boson system,

$$H = H_0 + \sum_j \frac{p_j^2}{2} + \frac{1}{2}\omega_j^2 x_j^2 - c_j x_j \sigma_z, \tag{11}$$

$$H_0 = \sigma_z - \sigma_x, \tag{12}$$

where $\sigma_{x/z}$ are the Pauli spin matrices. The bath interacts with the σ_z system operator and is characterized by a Drude spectral density,

$$J(\omega) = \frac{\lambda\gamma\omega}{2(\omega^2+\gamma^2)}, \tag{13}$$

where the reorganization energy $\lambda = 1.5$ and the cutoff frequency $\gamma = 7.5$. The simulations are done at an inverse temperature of $\beta = 2.0$. The bath is discretized into 50 oscillators. For the quantum–classical methods, a 100 000 Monte Carlo points are used for sampling the Wigner distribution. The simulations were run with a time-step of $\Delta t = 0.1$ (The change in the dynamics with the number of oscillators is shown in Appendix B).

We demonstrate the route of convergence of QC-HEOM to the QuAPI results and compare it with QCPI results with a free solvent (or EACP) reference. The convergence with respect to the number of Monte Carlo samples and the number of oscillators is going to be similar because both the methods separate the influence functional in the same way. The major difference is that QCPI truncates the quantum memory beyond K time-steps, whereas QC-HEOM captures the full quantum memory at different levels of accuracy given

15 November 2026 03:50:56

Published under an exclusive license by AIP Publishing

by the depth of the hierarchy, L. QCPI becomes exact as K gets larger, and QC-HEOM becomes exact as L becomes larger. Here, we compare the convergence of QCPI with respect to K and QC-HEOM with respect to L.

The results are shown in Fig. 1. First, note that QC-HEOM reproduces the EACP results at $L = 0$. This corresponds to the $K = 0$ EACP run for QCPI. QCPI shows a gradual convergence to the QuAPI results (shown in black markers) with memory length K. It is well-known that using a dynamically consistent state-hopping[30] (DCSH) reference can speed up convergence, capturing effects of the asymmetry even at $K = 0$ levels. Coming to the QC-HEOM convergence, though it is controlled by the depth of hierarchy and not the memory length, we see certain qualitatively different features. Increasing the hierarchy depth from $L = 0$ to $L = 1$ remarkably is already sufficient to obtain near-quantitative agreement with the QuAPI benchmark. In Fig. 2, we demonstrate the dynamics of the off-diagonals of the reduced density matrix in terms of the time-evolution of $\langle\sigma_x(t)\rangle$ and $\langle\sigma_y(t)\rangle$. While $\langle\sigma_x(t)\rangle$ shows a convergence very similar to that of $\langle\sigma_z(t)\rangle$, the overall error in $\langle\sigma_y(t)\rangle$ is much less than the other two Pauli spin operators. This is probably because the σ_y is related to the population flux and has to go to zero at long times. We do notice that the $L = 0$ curve is distinctly different from the $L = 1$ and higher curves.

Till now, we have demonstrated observables that are linear in the RDM. To make the simulation more challenging, we now plot the von Neumann entropy,

$$S[\tilde{\rho}(t)] = -\,\mathrm{Tr}\,[\tilde{\rho}(t)\log(\tilde{\rho}(t))], \tag{14}$$

which captures the time-evolution of the entanglement entropy between the system and the environment. In Fig. 3, we plot the entanglement entropy as obtained by QCPI and QC-HEOM at different stages of convergence. This is clearly more difficult to converge than the previous observables for both methods. The difference between $L = 1$, $L = 2$, and $L = 3$ is visible, though the approach to convergence is obvious.

At $L = 0$, QC-HEOM solves the equation of motion for a single 2×2 AQIF. Because there is only a single Drude bath, the imaginary part of the bath response function can be represented by a single exponential. Therefore, the $L = 1$ calculation only needs to solve coupled differential equations involving two 2×2 AQIFs. Finally, at $L = 2$, the differential equations involve three AQIFs.

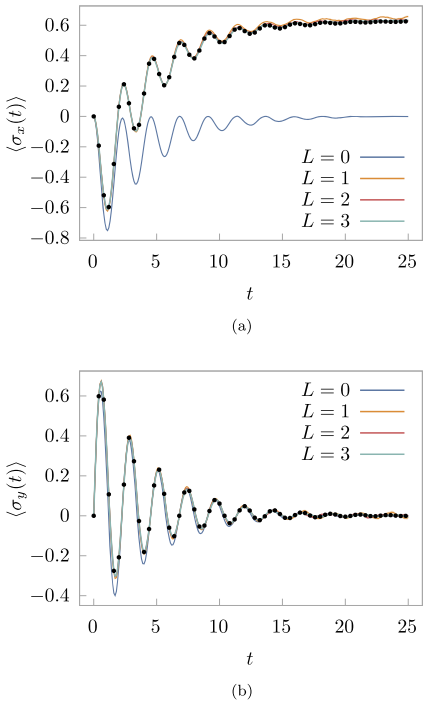


FIG. 2. Coherence dynamics in terms of $\langle\sigma_x(t)\rangle$ and $\langle\sigma_y(t)\rangle$ using QC-HEOM. (a) $\langle\sigma_x(t)\rangle$. (b) $\langle\sigma_y(t)\rangle$.

The rapid convergence with hierarchy depth reflects a fundamental difference between the two approaches. QCPI approximates the bath memory by truncating the influence functional after K timesteps, whereas QC-HEOM encodes the bath memory through the hierarchy of auxiliary quantum influence functionals. Increasing L systematically improves the representation of non-Markovian effects without introducing an explicit memory cutoff. On the other hand, a standard HEOM simulation of this system also converged to the same result. However, as mentioned in Sec. II, it requires explicit incorporation of the Bose–Einstein distribution in terms of additional modes. Convergence was achieved with 6 modes and a depth of $L = 4$, which resulted in 330 2×2 auxiliary density operators.

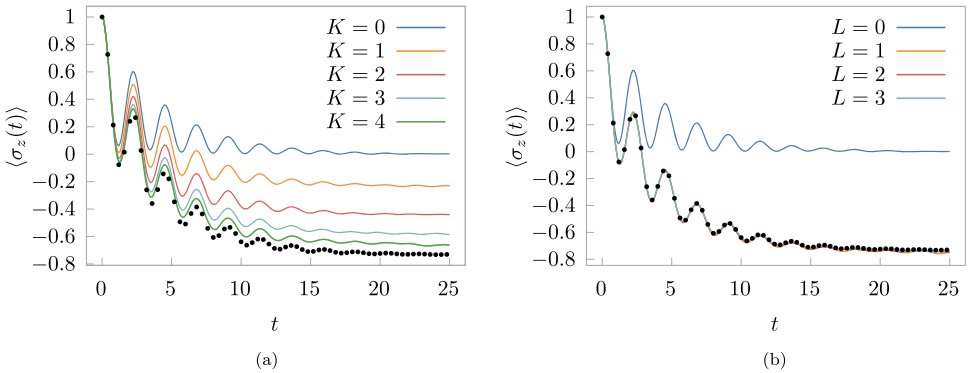


FIG. 1. Comparison of convergence of EACP-reference QCPI and QC-HEOM for the spin–boson model. Black markers: Converged QuAPI results. (a) EACP reference QCPI $\langle\sigma_z(t)\rangle$. (b) QC-HEOM $\langle\sigma_z(t)\rangle$.

15 November 2026 03:50:56

Published under an exclusive license by AIP Publishing

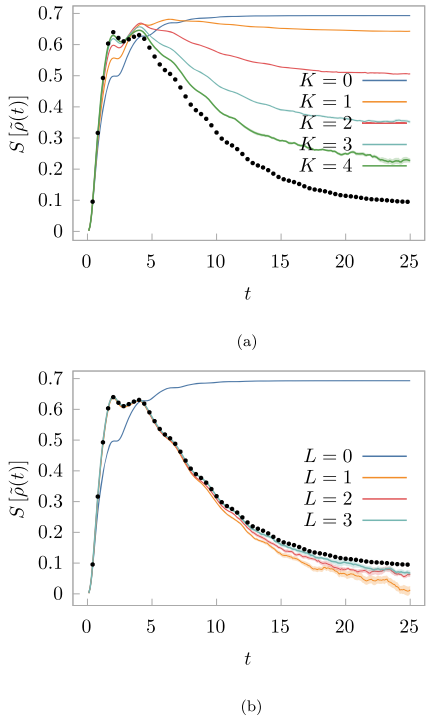


FIG. 3. Convergence of the von Neumann entropy for QCPI and QC-HEOM. Black markers are converged path integral results. (a) Von Neumann entropy at different QCPI memory lengths. (b) Von Neumann entropy at different QC-HEOM hierarchy depths.

As an example with a more involved spectral density, consider a spectral density that is given as a sum of a Drude–Lorentz and an underdamped Brownian oscillator,

$$J(\omega) = \frac{\lambda_D \gamma_D \omega}{2(\omega^2 + \gamma_D^2)} + \frac{\lambda_U \gamma_U \omega_0^2 \omega}{2((\omega^2 - \omega_0^2)^2 + \gamma_U^2 \omega^2)}, \tag{15}$$

where λ_D and λ_U are the reorganization energies corresponding to the Drude–Lorentz and the underdamped Brownian baths, respectively, γ_D and γ_U are their respective time-scales, and ω_0 is the center of the underdamped oscillator. The combined bath interacts with the σ_z operator of the system. One can think of this as modeling an unstructured bath with a single important frequency. For the first example, we simulated $\lambda_D = 10\lambda_U = 1.5$, yielding a total reorganization energy of 1.65. The timescales were chosen to be $\gamma_D = 7.5$ and $\gamma_U = 0.75$, and $\omega_0 = 3.75$. The resultant spectral density and the dynamics are shown in Fig. 4. We once again see the characteristic convergence of QC-HEOM at very low depths of the hierarchy. A value of $L = 2$ is completely converged, with $L = 1$ capturing all the physically relevant properties but slightly overestimating the long time oscillations. In contrast, the path integral simulations required extremely long memory lengths owing to the underdamped Brownian oscillator. The time-evolving matrix product operators algorithm[5] was used, and convergence was achieved at a memory length of 60 time-steps.

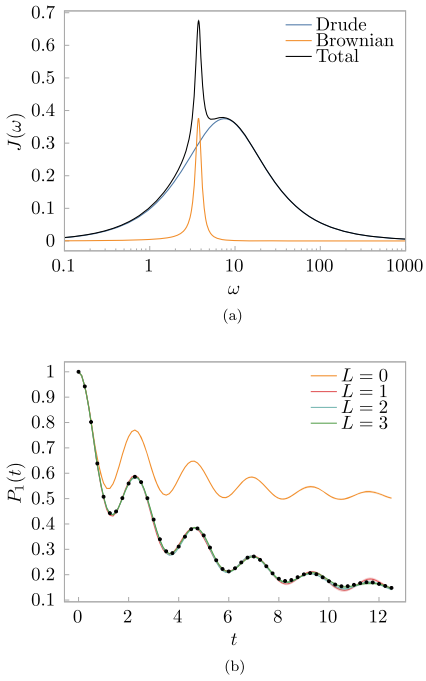


FIG. 4. Composite spectral density and the corresponding dynamics. Black markers are converged path integral results with 60 steps of memory. (a) Composite spectral density. (b) Dynamics.

B. Fenna–Matthews–Olson complex

The Fenna–Matthews–Olson complex is a widely studied trimeric pigment–protein complex involved in photosynthetic exciton transport, with each monomer containing eight bacteriochlorophyll molecules (also referred to as sites). We consider the single-excitation manifold of an individual monomer, modeled using a Frenkel exciton Hamiltonian,

$$H_0 = \sum_{j=1}^{8} \epsilon_j |j\rangle\langle j| + \sum_{j=1}^{8} \sum_{k=j+1}^{8} h_{jk}(|j\rangle\langle k| + |k\rangle\langle j|), \tag{16}$$

where $|j\rangle$ represents the state of the system with the jth molecule in the excited state and all others in the ground state. The energy of the excited state of the jth molecule is ϵ_j, and the coupling of the jth and kth molecule is h_{jk}. We use the site-energies and intersite couplings as reported in Ref. 35. The molecular vibrations and the motion of the protein scaffolding provide a thermal dissipative environment modifying the exciton transport. This is built in as local harmonic baths on each of the monomers,

$$H = H_0 + \sum_{j=1}^{8} \sum_{l} \left(\frac{p_{jl}^2}{2} + \frac{1}{2}\omega_{jl}^2 x_{jl}^2 - c_{jl} x_{jl} |j\rangle\langle j| \right). \tag{17}$$

The frequency and coupling of the lth oscillator of the bath on the jth monomer are ω_{jl} and c_{jl}, respectively. Following Ref. 35, we use Drude–Lorentz spectral densities $\left(J_j(\omega) = \frac{2\lambda_j \gamma_j \omega}{\omega^2 + \gamma_j^2}\right)$ for each of the eight baths. However, each bath has a different reorganization

15 November 2026 03:50:56

Published under an exclusive license by AIP Publishing

energy and cutoff frequency, with the average reorganization energy being $\lambda = 102\ \mathrm{cm}^{-1}$.[35] We demonstrate the QC-HEOM method on this system. Each bath is discretized into 50 oscillators, and 40 000 Monte Carlo points are used for sampling the Wigner distribution. In the QC-HEOM treatment, owing to the Drude–Lorentz nature of the baths, each bath response function is represented as a single exponential. This implies that the number of AQIFs used at a hierarchy depth of L is $N_{\mathrm{AQIF}}(L) = \left(\frac{N_{\mathrm{sites}}+L}{L}\right)$, where N_{sites} is the number of sites or molecules and is equal to 8 in this case. Simulations are carried out at three different temperatures: (a) physiological temperature of 300 K, (b) liquid nitrogen temperature of 77 K, and (c) 10 K.

We start by evaluating the convergence of the system at the three temperatures. To clearly visualize the convergence, we focus only on the dynamics of the sites 1–4 at different values of L, as shown in Fig. 5. The $L = 0$ simulation, of course shows the least accurate results at all temperatures, with the long-time limit going to a value of $\frac{1}{8}$ for every monomer. Though the EACP results account for the full classical memory, they do not capture the backreaction and tend to mimic a high-temperature limit. This makes the difference in the site-energies insignificant, leading to equal long-time populations. On increasing the value of L, we immediately see the difference between the monomers start to show up. The convergence with respect to L, while not as fast as the spin–boson systems in Sec. III A, is still quite rapid, with the convergence being reached at $L = 3$ at all three temperatures. In the low temperature cases of $T = 77$ K and $T = 10$ K, it is clear that the convergence of the QC-HEOM calculations does not happen in a monotonic manner, and the change from the $L = 1$ to the $L = 2$ run seems to take the dynamics away from the converged results, before the dynamics converges at $L = 3$, which requires 165 AQIFs. Within Monte Carlo statistical uncertainties associated with the sampling of the Wigner distribution, the dynamics is identical for depths of hierarchy, L, from 3 to 5. This kind of a pattern was also observed in an example simulated by stochastic HEOM.[16]

Next, let us consider the approximate per-initial condition runtime and the number of AQIFs used at different depths of the hierarchy for this problem. These are shown in Fig. 6. It must be acknowledged that the timings are from a preliminary version of the code, and several further optimizations are indeed possible. Additionally, run-times are highly dependent on the processor on which the calculation is run. The current benchmarks were run using a dual-socket Intel Xeon Platinum 8176 server. This graph should only be used as a way to understand how the run-time changes at different levels of the hierarchy. We plot only the per-initial condition cost in view of the embarrassingly parallel nature of the different initial conditions. All differential equations are integrated using the adaptive Tsitouras Runge–Kutta method,[36] with absolute and relative tolerances of 10^{-8} and 10^{-6}, respectively. The scaling of per initial condition run-time with L is consistent with the number of AQIFs used at a particular level of L. Moreover, at $T = 300$ K, the thermal Wigner distribution samples many more trajectories with higher energies than the $T = 77$ K or the $T = 10$ K simulation. As a result of this, one might imagine that a smaller classical time-step will be required, leading to an increase in the overall cost of simulation at higher temperatures. However, because of the analytical trajectories of harmonic oscillators, this does not create a measurable difference in the actual run-time.

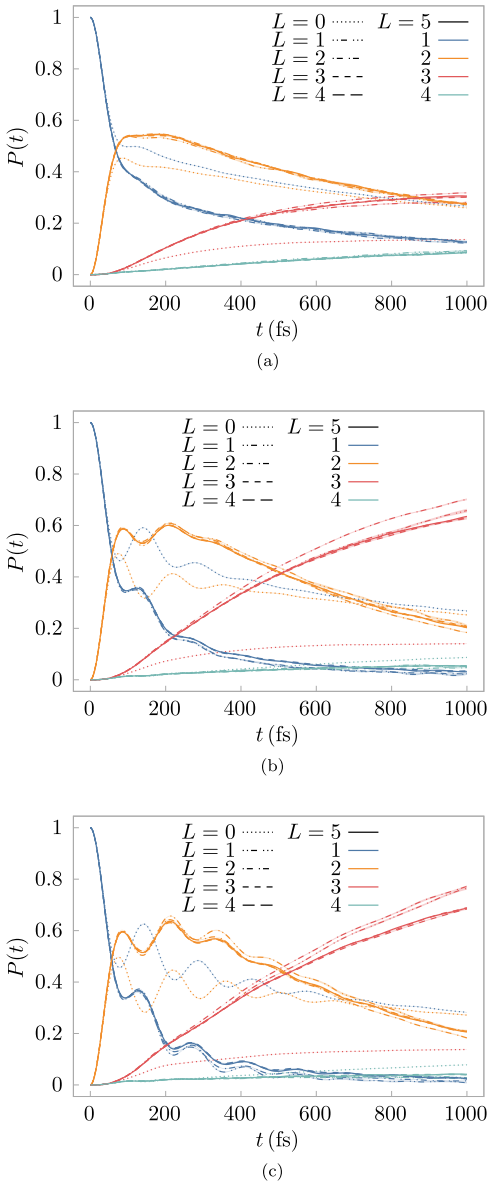


FIG. 5. Dynamics of the FMO at different temperatures. The dash types represent different L simulations, and the color shows the dynamics of the monomers. (a) Dynamics at 300 K. (b) Dynamics at 77 K. (c) Dynamics at 10 K.

Finally, we estimate the hierarchy-truncation error at a given depth L by comparing the population dynamics with those obtained using an $(L+1)$-level hierarchy. The error in the population of the jth molecule at the Lth level, relative to the $(L+1)$th level, is computed as a root-mean-square (RMS) deviation of the populations across the entire time-span of the simulation,

$$\Delta_j^{(L)} = \sqrt{\frac{1}{t_{\mathrm{fin}}}\int_0^{t_{\mathrm{fin}}} \left(\left\langle j\middle|\tilde{\rho}^{(L+1)}\middle|j\right\rangle - \left\langle j\middle|\tilde{\rho}^{(L)}\middle|j\right\rangle\right)^2}, \tag{18}$$

15 November 2026 03:50:56

Published under an exclusive license by AIP Publishing

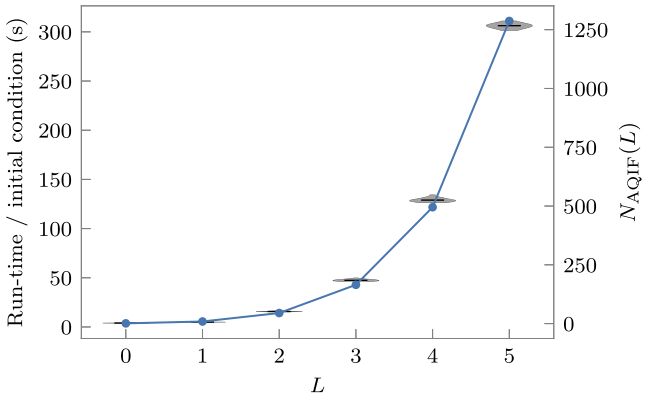


FIG. 6. Per initial condition timing and number of AQIFs. Timing: violin plot on the left *y*-axis, number of AQIFs: line plot on the right *y*-axis.

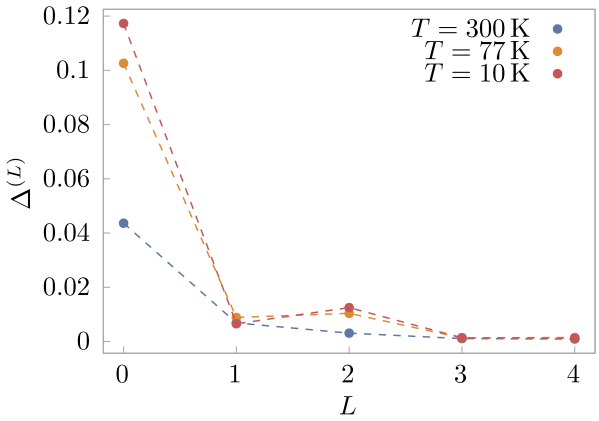


FIG. 7. Error corrected in going from an Lth order calculation to an $(L+1)$th order calculation.

where $t_{\mathrm{fin}} = 1$ ps is the final time of the simulation done. We use the average per-site RMS error, $\Delta^{(L)} = \frac{1}{8}\sum_{j=1}^{8}\Delta_j^{(L)}$, as a global measure of the convergence. This error is shown in Fig. 7. Similar to the spin–boson examples in Sec. III A, the majority of the corrections are accounted for in going from $L = 0$ to $L = 1$. In this case, given the higher reorganization energy of the baths, substantial corrections happen at $L = 1$ and $L = 2$ levels as well. Within the statistical uncertainty associated with the Monte Carlo sampling, $\Delta^{(L)}$ vanishes for $L \geq 3$, demonstrating convergence of the population dynamics with respect to hierarchy depth.

IV. CONCLUSION

Quantum–classical path integrals provide a rigorous framework for approximating non-Markovian quantum dynamics in complex environments by separating the influence of classical solvent fluctuations from the residual quantum memory. In this framework, the ensemble-averaged classical path (EACP) reference propagators incorporate the contribution of the real part of the bath response function through solvent-driven trajectories, while the remaining quantum influence function retains the non-classical backreaction. However, despite the reduction in effective quantum memory, QCPI still requires the evaluation of a path integral for each sampled solvent trajectory, which can become computationally prohibitive for large systems.

In this work, we have introduced quantum–classical hierarchical equations of motion (QC-HEOM), which combines the reference trajectory formulation of QCPI with a hierarchical representation of the residual quantum influence functional. By explicitly separating the classical and quantum contributions to the bath response, QC-HEOM replaces the repeated path-integral evaluation of the quantum influence function with a hierarchy of coupled auxiliary quantum influence functionals. For harmonic environments, this construction provides a formally exact reformulation of the residual quantum memory and is equivalent to the underlying QuAPI description.

A central consequence of this separation is that the hierarchy is constructed only from the temperature-independent residual backreaction kernel. Unlike conventional HEOM, where the thermal component of the bath correlation function requires a Matsubara or Padé decomposition, QC-HEOM incorporates thermal fluctuations entirely through the ensemble of Wigner trajectories. Consequently, the hierarchy size exhibits only weak temperature dependence and is determined primarily by the physical poles of the spectral density rather than by the poles required to represent the Bose–Einstein distribution. This removes one of the primary sources of low-temperature complexity in standard HEOM.

The performance of QC-HEOM was demonstrated for an asymmetric spin–boson model and an 8-site model of the Fenna–Matthews–Olson complex over a broad range of temperatures. In both cases, convergence was achieved at very low depths of the hierarchy. Moreover, because of the lack of Matsubara or Padé modes for incorporating the thermal contributions, the number of auxiliary quantum influence functions that are propagated is extremely small. For the spin–boson examples, convergence was seen at $L = 1$, while for the FMO calculations, owing to a much higher system-bath reorganization energy, convergence was achieved for $L \geq 3$. The only additional cost stems from the multiple calculations being performed for every Monte Carlo sample. This too is embarrassingly parallelizable across multiple processors.

An important feature of QC-HEOM is that the hierarchy is not intrinsically limited to a particular choice of reference dynamics. The present work employs the EACP reference because it provides an exact separation of classical and quantum memory for harmonic baths. However, more physically motivated reference trajectories may further reduce the residual quantum contribution that must be represented hierarchically. In particular, exploring trajectories generated from mean-field approaches such as Ehrenfest dynamics, or the dynamically consistent state-hopping Ref. 30 seem to be promising choices. Such optimized reference propagators could shift additional environmental effects from the quantum hierarchy into the classical trajectory ensemble, thereby reducing the required hierarchy depth while retaining a systematic treatment of residual quantum memory.

15 November 2026 03:50:56

Published under an exclusive license by AIP Publishing

The present formulation focuses on harmonic environments, where the QC-HEOM construction is formally exact. Nevertheless, the trajectory-based nature of the method provides a natural route toward extensions involving anharmonic and atomistic environments. Similar to QCPI, reference trajectories generated from molecular simulations or *ab initio* dynamics could be incorporated, while the remaining quantum backreaction could be treated using suitable approximations such as harmonic mappings or improved semiclassical corrections.[26,27] The development of physically optimized reference trajectories and systematic approximations for anharmonic residual memory represent important directions for future work.

Finally, the hierarchical structure introduced here is complementary to recent developments in HEOM methodology, including generalized exponential decompositions and free-pole representations,[13] tensor-network representations of the hierarchy,[37] and other approaches for reducing the complexity of large auxiliary spaces. Combining these developments with the quantum–classical separation introduced in QC-HEOM may enable simulations of larger molecular and condensed-phase systems with structured and anharmonic environments.

Overall, QC-HEOM provides a new perspective on hierarchical open-system dynamics by treating classical environmental fluctuations through trajectory ensembles while reserving the hierarchy for the genuinely quantum component of the environmental memory. This separation offers a promising framework for combining the accuracy of numerically exact methods with the flexibility of trajectory-based approaches for increasingly complex quantum dynamical systems.

AUTHOR DECLARATIONS

Conflict of Interest

The authors have no conflicts to disclose.

Author Contributions

Amartya Bose: Conceptualization (lead); Data curation (lead); Formal analysis (lead); Funding acquisition (lead); Investigation (lead); Methodology (lead); Software (lead); Validation (lead); Visualization (lead); Writing – original draft (lead); Writing – review & editing (lead).

DATA AVAILABILITY

The data that support the findings of this study are available from the corresponding author upon reasonable request.

APPENDIX A: EXPONENTIAL REPRESENTATION OF THE TEMPERATURE-INDEPENDENT BATH KERNEL

For a general spectral density, $J(\omega)$, the bath response function, $\alpha(t)$ given by Eq. (4), governs HEOM, which proceeds to decompose it in terms of exponentials. In QC-HEOM, $\mathrm{Re}\,\alpha(t)$ is fully incorporated through the classical trajectories initialized on the thermal Wigner distribution for the bath. It then requires exponential decompositions of the $C_{\mathrm{back}}(t)$. While the current implementation uses a more traditional HEOM-like backend, the concept of QC-HEOM, by itself, is not limited to such a treatment. As mentioned in the main body of the paper, ideas of barycentric representations using the AAA algorithm[31] or other rational fittings for more general spectral densities, as employed by the free-pole HEOM,[13] can be adapted for $C_{\mathrm{back}}(t)$ in the future. This will allow QC-HEOM to be systematically extended to an even broader class of spectral densities.

In terms of model spectral densities, we have already mentioned that for the Ohmic form with a Lorentzian tail, conventionally called the Drude–Lorentz spectral density, $C_{\mathrm{back}}(t)$ is a single exponential with real poles. Here, we discuss the decompositions of $C_{\mathrm{back}}(t)$ for some common types of model spectral densities. For an Ohmic spectral density with a Lorentzian decay, or what is traditionally called a Drude–Lorentz spectral density, one can show that $C_{\mathrm{back}}(t)$ can be represented as a single exponential decay,

$$J^{\mathrm{ohmic}}(\omega) = \frac{2\lambda\gamma}{\Delta s^2}\frac{\omega}{\omega^2+\gamma^2}, \tag{A1}$$

$$C^{\mathrm{ohmic}}_{\mathrm{back}}(t) = -i\frac{\lambda\gamma}{\Delta s^2}\exp(-\gamma t). \tag{A2}$$

Now consider a more general family of spectral densities, all with the Lorentzian cutoff,

$$J^{(s)}(\omega) = \frac{2\lambda\gamma^{2-s}}{\Delta s^2}\sin\left(\frac{\pi s}{2}\right)\frac{\omega^s}{\omega^2+\gamma^2}, \tag{A3}$$

for $s > 0$, where $s = 1$ reduces to the familiar Ohmic case, and $0 < s < 1$ are their sub-Ohmic counterparts. The set of spectral densities generated by using $s > 1$ seems to generate a family of super-Ohmic spectral densities. The Lorentzian-cutoff family generated here is not suitable for physically meaningful super-Ohmic spectral densities because its reorganization energy diverges for $s > 1$. Realistic super-Ohmic environments instead employ rapidly decaying high-frequency cutoffs, such as Gaussian or exponential, or experimentally parameterized spectral densities.

In contrast to the Ohmic Drude–Lorentz, these sub-Ohmic cases do not lead to simplification in the sense that the bath response function can be represented by a single pole. There are two contributions to $C_{\mathrm{back}}(t)$, one from the pole and the other from a branch cut. This latter part is not exponential but polynomial in t,

$$C^{s}_{\mathrm{back}}(t) = -i\frac{\lambda\gamma}{\Delta s^2}\sin^2\left(\frac{\pi s}{2}\right)\exp(-\gamma t) - i\frac{2\lambda\gamma^{2-s}}{\pi\Delta s^2}\Gamma(s+1)\sin\left(\frac{\pi s}{2}\right)\sin(\pi s)t^{-(s+1)}. \tag{A4}$$

The first term is an exponential decay and fits our requirement. Now for QC-HEOM, the second term needs to be expanded in terms of exponentials. Laplace transforming the algebraic tail, we get

$$t^{-(s+1)} = \frac{1}{\Gamma(s+1)}\int_0^\infty \Lambda^s \exp(-\Lambda t)\mathrm{d}\Lambda. \tag{A5}$$

So one can in principle simply discretize the integral into several modes through a quadrature representation. However, a naïve linear grid quadrature would involve a proliferation of the number of modes. A more optimal approach is to use a logarithmic

15 November 2026 03:50:56

Published under an exclusive license by AIP Publishing

discretization by assuming $\Lambda = \exp(x)$ and consequently $d\Lambda = \exp(x)dx$. Now, x can be uniformly discretized, resulting in a geometric spacing of the Λ points. The final controlled exponential decomposition of the algebraic tail using this discretization, therefore, is

$$x_k = x_{\min} + k\Delta x, \tag{A6}$$

$$\Lambda_k = \exp(x_k), \tag{A7}$$

$$t^{-(s+1)} = \sum_{k=1}^{N} \frac{\Delta x}{\Gamma(s+1)} \Lambda_k^{s+1} \exp(-\Lambda_k t). \tag{A8}$$

Thus, although the sub-Ohmic kernel is not represented exactly by a finite number of exponential terms, it admits a systematically improvable exponential expansion through quadrature of the Laplace representation.

For the Brownian baths, where

$$J(\omega) = \frac{2\lambda}{\Delta s^2} \frac{\gamma\omega_0^2\omega}{\left(\omega^2 - \omega_0^2\right)^2 + \gamma^2\omega^2}, \tag{A9}$$

the residual bath response function is expanded as a sum over two exponentials. If we define $\Omega = \sqrt{\omega_0^2 - \frac{\gamma^2}{4}}$, then the residual bath response function,

$$C_{\text{back}}(t) = -\frac{\lambda\omega_0^2}{2\Delta s^2\Omega}\left(e^{-\left(\frac{\gamma}{2}-i\Omega\right)t} - e^{-\left(\frac{\gamma}{2}+i\Omega\right)t}\right). \tag{A10}$$

This holds so long as $\Omega \neq 0$, with $\Omega \in \mathbb{R}$ characterizing the underdamped cases, and purely imaginary Ωs characterizing overdamped cases. For the underdamped Brownian bath, the poles are conjugates of each other, whereas they just become two distinct real exponential decays for the overdamped case. If $\gamma = 2\omega_0$, there is a double pole, which does not have a simple exponential representation. This critical damping case therefore requires a slight modification of the hierarchy analogous to the treatment of repeated poles in generalized HEOM formulations.

APPENDIX B: CONVERGENCE OF SPIN–BOSON DYNAMICS WITH NUMBER OF OSCILLATORS

For quantum–classical hierarchical equations of motion, as in other quantum–classical methods, one needs to discretize the baths. Like any of the harmonic back-reaction architectures,[26] this discretization only affects the classical memory part, while the quantum memory is included completely through either the influence functional[8,27] or through hierarchy of equations of motion in this case. This is unlike other semiclassical and quasiclassical methods,[38–40] where all the components of dynamics is affected by the bath discretization. In Fig. 8, we show the convergence of various observables with the number of oscillators for the asymmetric spin–boson with a Drude–Lorentz spectral density explored in Fig. 1. Calculations are run at $L = 2$ with 10, 20, 30, 40, and 50

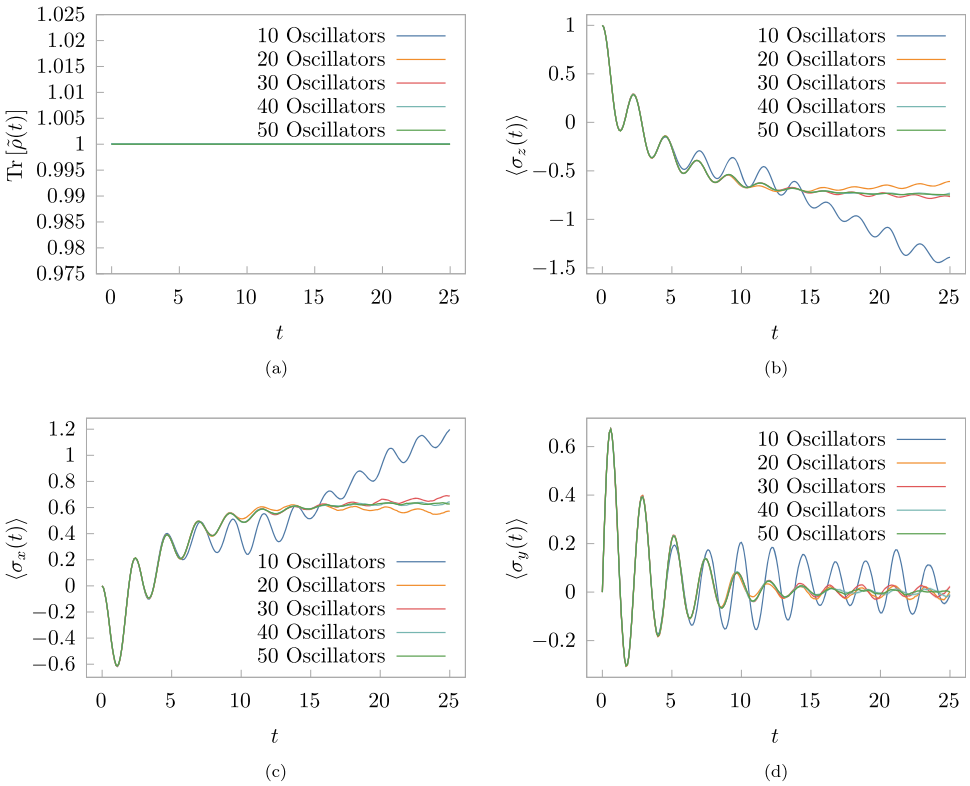


FIG. 8. Convergence of dynamics with respect to the number of oscillators. (a) Conservation of trace. (b) Convergence of σ_z. (c) Convergence of σ_x. (d) Convergence of σ_y.

15 November 2026 03:50:56

Published under an exclusive license by AIP Publishing

oscillators. First, we see in Fig. 8(a), the trace conservation holds for all number of oscillators. The expectation value of the other Pauli matrices seems to stabilize by 40 oscillators. The errors due to the finite number of oscillators grow with time. So, if one focuses on $t \leq 5$, then probably even 10 oscillators is enough, though at longer times, it clearly shows signs of recurrence.

REFERENCES

[1] N. Makri and D. E. Makarov, "Tensor propagator for iterative quantum time evolution of reduced density matrices. I. Theory," J. Chem. Phys. **102**, 4600–4610 (1995).

[2] N. Makri and D. E. Makarov, "Tensor propagator for iterative quantum time evolution of reduced density matrices. II. Numerical methodology," J. Chem. Phys. **102**, 4611–4618 (1995).

[3] N. Makri, "Blip decomposition of the path integral: Exponential acceleration of real-time calculations on quantum dissipative systems," J. Chem. Phys. **141**, 134117 (2014).

[4] N. Makri, "Iterative blip-summed path integral for quantum dynamics in strongly dissipative environments," J. Chem. Phys. **146**, 134101 (2017).

[5] A. Strathearn, P. Kirton, D. Kilda, J. Keeling, and B. W. Lovett, "Efficient non-Markovian quantum dynamics using time-evolving matrix product operators," Nat. Commun. **9**, 3322 (2018).

[6] A. Bose, "Pairwise connected tensor network representation of path integrals," Phys. Rev. B **105**, 024309 (2022).

[7] A. Bose and P. L. Walters, "A multisite decomposition of the tensor network path integrals," J. Chem. Phys. **156**, 024101 (2022).

[8] R. P. Feynman and F. L. Vernon, "The theory of a general quantum system interacting with a linear dissipative system," Ann. Phys. **24**, 118–173 (1963).

[9] Y. Tanimura and R. Kubo, "Time evolution of a quantum system in contact with a nearly Gaussian-Markoffian noise Bath," J. Phys. Soc. Jpn. **58**, 101–114 (1989).

[10] A. Ishizaki and Y. Tanimura, "Quantum dynamics of system strongly coupled to low-temperature colored noise bath: Reduced hierarchy equations approach," J. Phys. Soc. Jpn. **74**, 3131–3134 (2005).

[11] Y. Tanimura, "Stochastic Liouville, Langevin, Fokker–Planck, and master equation approaches to quantum dissipative systems," J. Phys. Soc. Jpn. **75**, 082001 (2006).

[12] Q. Shi, L. Chen, G. Nan, R.-X. Xu, and Y. Yan, "Efficient hierarchical Liouville space propagator to quantum dissipative dynamics," J. Chem. Phys. **130**, 084105 (2009).

[13] M. Xu, Y. Yan, Q. Shi, J. Ankerhold, and J. T. Stockburger, "Taming quantum noise for efficient low temperature simulations of open quantum systems," Phys. Rev. Lett. **129**, 230601 (2022).

[14] Y. Tanimura, "Real-time and imaginary-time quantum hierarchal Fokker-Planck equations," J. Chem. Phys. **142**, 144110 (2015).

[15] Y. Tanimura, "Numerically 'exact' approach to open quantum dynamics: The hierarchical equations of motion (HEOM)," J. Chem. Phys. **153**, 020901 (2020).

[16] J. M. Moix and J. Cao, "A hybrid stochastic hierarchy equations of motion approach to treat the low temperature dynamics of non-Markovian open quantum systems," J. Chem. Phys. **139**, 134106 (2013).

[17] Y. Ke and Y. Zhao, "An extension of stochastic hierarchy equations of motion for the equilibrium correlation functions," J. Chem. Phys. **146**, 214105 (2017).

[18] J. C. Tully, "Mixed quantum–classical dynamics," Faraday Discuss. **110**, 407–419 (1998).

[19] J. C. Tully, "Molecular dynamics with electronic transitions," J. Chem. Phys. **93**, 1061–1071 (1990).

[20] J. C. Tully, "Nonadiabatic molecular dynamics," Int. J. Quantum Chem. **40**, 299–309 (1991).

[21] J. C. Tully, "Perspective: Nonadiabatic dynamics theory," J. Chem. Phys. **137**, 22A301 (2012).

[22] R. Lambert and N. Makri, "Quantum-classical path integral. I. Classical memory and weak quantum nonlocality," J. Chem. Phys. **137**, 22A552 (2012).

[23] R. Lambert and N. Makri, "Quantum-classical path integral. II. Numerical methodology," J. Chem. Phys. **137**, 22A553 (2012).

[24] T. Banerjee and N. Makri, "Quantum-classical path integral with self-consistent solvent-driven reference propagators," J. Phys. Chem. B **117**, 13357–13366 (2013).

[25] N. Makri, "Quantum-classical path integral: A rigorous approach to condensed phase dynamics," Int. J. Quantum Chem. **115**, 1209–1214 (2015).

[26] F. Wang and N. Makri, "Quantum-classical path integral with a harmonic treatment of the back-reaction," J. Chem. Phys. **150**, 184102 (2019).

[27] A. Bose, "Phase space and path integral approaches to quantum dynamics," Ph.D. thesis, University of Illinois, Urbana-Champaign, Urbana, 2018.

[28] C.-Y. Hsieh and J. Cao, "A unified stochastic formulation of dissipative quantum dynamics. II. Beyond linear response of spin baths," J. Chem. Phys. **148**, 014104 (2018).

[29] C.-Y. Hsieh and J. Cao, "A unified stochastic formulation of dissipative quantum dynamics. I. Generalized hierarchical equations," J. Chem. Phys. **148**, 014103 (2018).

[30] P. L. Walters and N. Makri, "Iterative quantum-classical path integral with dynamically consistent state hopping," J. Chem. Phys. **144**, 044108 (2016).

[31] Y. Nakatsukasa, O. Sète, and L. N. Trefethen, "The AAA algorithm for rational approximation," SIAM J. Sci. Comput. **40**, A1494–A1522 (2018).

[32] J. Hu, R.-X. Xu, and Y. Yan, "Communication: Padé spectrum decomposition of Fermi function and Bose function," J. Chem. Phys. **133**, 101106 (2010).

[33] J. Hu, M. Luo, F. Jiang, R.-X. Xu, and Y. Yan, "Padé spectrum decompositions of quantum distribution functions and optimal hierarchical equations of motion construction for quantum open systems," J. Chem. Phys. **134**, 244106 (2011).

[34] A. Bose, "QuantumDynamics.jl: A modular approach to simulations of dynamics of open quantum systems," J. Chem. Phys. **158**, 204113 (2023).

[35] X. Jia, Y. Mei, J. Z. H. Zhang, and Y. Mo, "Hybrid QM/MM study of FMO complex with polarized protein-specific charge," Sci. Rep. **5**, 17096 (2015).

[36] C. Tsitouras, "Runge–Kutta pairs of order 5(4) satisfying only the first column simplifying assumption," Comput. Math. Appl. **62**, 770–775 (2011).

[37] X. Chen and I. Franco, "Tree tensor network hierarchical equations of motion based on time-dependent variational principle for efficient open quantum dynamics in structured thermal environments," J. Chem. Phys. **163**, 104109 (2025).

[38] H. Wang, X. Sun, and W. H. Miller, "Semiclassical approximations for the calculation of thermal rate constants for chemical reactions in complex molecular systems," J. Chem. Phys. **108**, 9726–9736 (1998).

[39] P. Huo and D. F. Coker, "Communication: Partial linearized density matrix dynamics for dissipative, non-adiabatic quantum evolution," J. Chem. Phys. **135**, 201101 (2011).

[40] J. R. Mannouch and J. O. Richardson, "A partially linearized spin-mapping approach for nonadiabatic dynamics. I. Derivation of the theory," J. Chem. Phys. **153**, 194109 (2020).

15 November 2026 03:50:56

Published under an exclusive license by AIP Publishing